Journal of Sound and Vibration 329 (2010) 753–767

Contents lists available at ScienceDirect

Journal of Sound and Vibration

journal homepage: www.elsevier.com/locate/jsvi

Optimising open porous foam for acoustical and vibrational performance

Eleonora Lind-Nordgren *, Peter Göransson

KTH Aeronautical and Vehicle Engineering, Marcus Wallenberg Laboratory of Sound and Vibration Research, SE-100 44 Stockholm, Sweden

ARTICLE INFO

Article history:
Received 23 February 2009
Received in revised form
26 August 2009
Accepted 8 October 2009
Handling Editor: Y. Auregan
Available online 31 October 2009

ABSTRACT

A computational method for designing optimal arrangements of multilayer noise and vibration treatments in general and porous open cell foam in particular is discussed. The method uses finite element solutions to Biot's equations for poroelastic materials and provides data to evaluate cost functions and gradients. The porous material is parameterised using scaling laws linking the microscopic properties to the classical parameters, i.e. averaged elasticity, flow resistivity and characteristic viscous and thermal lengths. The cost function is either in terms of weight or in terms of the pressure response in a finite cavity, complemented with constraints on the other. However, care must be taken when choosing the cost function, as this will greatly affect the outcome of the optimisation. Observations made during the optimisation process indicate a limited number of minima within the parameter range of interest as well as beneficial continuity around these minima, thus enabling a meaningful optimisation. The results suggest that if alterations of the microscopic properties of the foam are made, the foam may be adapted to specific environmental conditions and thereby achieve improved acoustic behaviour as well as reduced weight.

1. Introduction

Flexible porous foams with open cells are generally considered to be good sound absorbers and vibration isolators, and are therefore often used to improve the noise vibration and harshness (NVH) comfort, commonly in automotive applications. However, adding such materials in vehicles generally has a negative impact on the overall weight and consequently the fuel or energy consumption. Hence, it is necessary to achieve the best possible performance, per added weight and cost, from the added material. In current practice, efficient use of porous foam often involves multiple layers of various open cell foam, i.e. foam with different mechanical and material properties. Designing such complex structures, fulfilling various requirements, is at best a very time consuming task due to the extensive testing needed to achieve good results. Furthermore, there is also the question of defining the acoustic performance of a specific foam or combination of foam layers. At present, lightweight porous acoustic multilayer trim components are traditionally specified in terms of sound absorption and transmission loss. Foam that is developed according to this way of characterising their efficiency may, however, be sub-optimal in specific applications where for example structure borne sound is a major part of a vibration problem. Clearly there is a need for computational tools and procedures that are able to predict and optimise the behaviour of such multilayered structures. The present paper presents such a methodology for optimising porous layers in a multilayered configuration.

* Corresponding author. Tel.: +46 8 7907941; fax: +46 8 7906122.
E-mail address: eleonora@kth.se (E. Lind-Nordgren).

0022-460X/$ - see front matter © 2009 Elsevier Ltd. All rights reserved.
doi:10.1016/j.jsv.2009.10.009

Nomenclature

$b(\omega)$	frequency-dependent viscous drag parameter
c_g	pore shape dependent constant
C^ρ	foam dependent scaling constant for bulk density
C^σ	foam dependent scaling constant for static flow resistivity
C^E	foam dependent scaling constant for bulk E-modulus
d_s	average strut thickness of solid frame
E^s	Young's modulus for solid frame material
E^*	Young's modulus for homogenised foam
l_s	average strut length of solid frame
p	acoustic pressure
Q	dilatational coupling factor between fluid and solid frame
R	bulk modulus of fluid phase at zero solid frame dilatation
$\overline{u}_i^f$	Cartesian component of average fluid displacement
$\overline{u}_i^s$	Cartesian component of average solid displacement
α_∞	tortuosity
η	dynamic viscosity
λ	bulk Lamé's parameter at constant fluid pressure
$\hat{\lambda}$	bulk dynamic Lamé's
Λ	viscous characteristic length
Λ'	characteristic thermal length
μ	bulk Lamé's shear parameter
$\hat{\mu}$	bulk dynamic Lamé's shear parameter
ρ_a	inertial coupling factor, $\rho_a = -\rho_{12}$
ρ_f	density of fluid
ρ_s	density of solid frame material
ρ^*	bulk density of solid frame
σ^{static}	static flow resistivity of foam
ϕ	porosity, volume fraction of open pore fluid content
ω	frequency

In flexible porous foam, the vibroacoustic energy is carried both through the fluid in the pores (e.g. air) and through the solid frame material itself. The waves are strongly coupled and propagate simultaneously along the two phases with different amplitude and relative phase angle. Differences in amplitude and phase will transform some of the mechanical-acoustical energy into heat, mainly due to viscoelastic and viscoacoustic phenomena in the solid frame and at the interface between the solid frame and the fluid in the pores.

When modelling wave propagation through a porous medium, the foam is described as a homogenised continuum with co-existing solid and fluid phases with a coupled frame-fluid wave propagation—an approach commonly known as Biot's theory, see e.g. [1–3]. In Biot's theory the macroscopic space averaged properties of the foam, such as bulk density, porosity, flow resistivity and Young's modulus, are required. The dynamic behaviour is then presented as macroscopic space averaged quantities e.g. solid and fluid displacement, acoustic pressure, and elastic stress.

While known macroscopic properties can be used to derive the necessary macroscopic dynamic quantities appearing in Biot's equations, the former are inherently dependent on microscopic properties of the foam, such as geometry (e.g. pore size, strut length and strut thickness) as well as the actual material used for the solid frame. Thus improving the dynamic behaviour by optimising the macroscopic properties independently of one another is doubtful as it would most likely result in a foam that is impossible to realise physically. An alternative approach would be to use scaling laws that relate the macroscopic properties to the microscopic ones, where the latter may be changed independently. This is the approach taken in the current paper.

The objective of the present work is to establish a methodology to estimate the acoustic behaviour of porous foam as well as to explore the possibilities to optimise this behaviour. This is carried out by minimising a cost function when the foam is affected by an oscillating force or other acoustical phenomena. Another purpose of the paper is to show that alterations in the micromechanical properties of foam may have a significant effect on the acoustical behaviour and that, if these micromechanical properties could be controlled, foams could be tailored for specific needs. This may allow for NVH problems to be treated from another point of view than previously possible, i.e. design for application performance.

This paper will briefly review Biot's theory and a proposed set of parametric relations between microscopic structure and macroscopic homogenised properties that may be used in the formulation of a 3-D finite element model providing the response of a multilayered structure. In the model, a panel is connected to an air filled cavity, in a sub-volume of which the sound pressure level is evaluated for a given load. Results from optimisation of one layer in a multilayered configuration are discussed, in particular in view of the frequency weighting functions applied to evaluate the response and the influence the different weighting functions have on the optimal configuration found.

1.1. Related work

Optimising the performance of porous foams, modifying the microstructure geometry, has recently been discussed in the context of structural acoustic performance as well as acoustic absorption, targeting single and multilayer configurations.

Simon et al. [4] performed calculations of transmission loss resonance frequencies of a number of multilayered panels in order to determine the best layer combination. The material database originally consisted of several Nomex honeycomb, fibre glass, Kevlar, carbon and viscoelastic materials. The calculations suggested that due to the high stiffness of the included materials the resulting panel basically followed the mass law for the frequency band 500–5000 Hz and that the high damping provided by the viscoelastic layer was beneficial only at the coincidence frequency. Instead they proposed a solution using foams that are less stiff than e.g. honeycomb. Based on simulations of the transmission loss, which were partly validated in laboratory testing, the conclusion was that sandwich panels with open cell foam provide an adequate option for efficient noise applications.

Focusing on the actual optimisation routine, Tanneau et al. [5] discussed a method using genetic algorithms to optimise the layer combination, in terms of the number of layers and their respective thicknesses. Their optimisation was performed with materials chosen from a list of possible candidates. The list contains a limited number of solids, fluids and foam, where each foam is described with a set of material properties, among them: porosity, flow resistivity, tortuosity and Young's modulus. Such an optimisation may result in a well performing trim panel by using readily available foam, which is of course very attractive in most practical situations. This approach, however, requires previously known material parameters for each material that may be included in the multilayered configuration, a quite extensive and possibly costly measurement task. It also excludes the possibility of designing a new material for a specific task.

Lee et al. [6] performed a topology optimisation using the transfer matrix derived from Biot's equations to maximise the transmission loss. The authors used an MMA optimiser [7] to find the optimal layer sequence consisting of air layers and layers of a specific poroelastic material with fixed properties. The optimisation was performed at single frequencies as well as for narrow and wide frequency bands. The frequencies or frequency bands studied were all between 1 and 5 kHz. Results from the single frequency optimisation show that as the target frequency increases the number of layers increases. In addition the thickness of each layer decreases, partly due to constraints on the total thickness but mainly due to the shorter wavelengths that correspond to high frequencies. The results for single frequency optimisations were also compared with results of narrow band optimisations. As expected were the foams optimised for narrow band frequencies outperformed by the single frequency optimised foam at each individual frequency. The number of layers, however, increased as the upper and lower frequencies of the frequency band were increased, in agreement with the results from the single frequency optimisation.

Work that to some extent explored the influence of geometrical properties was performed by Franco et al. [8], who examined a sandwich panel with different core and face sheet properties. One configuration was a core made of a lattice of truss elements; this allowed independent control of the core stiffness along different directions. The truss like core was modelled as rod elements with the intent to minimise the mean square average inner surface velocity over a chosen frequency range. Their model, however, only regarded Young's modulus in different directions of a truss like unit cell by altering the cross-sectional area of the rod elements in different directions, whereas neither the coupled wave propagation due to the frame–fluid interaction, any of the well established energy dissipative mechanisms of foam nor the effects of damping levels with respect to different frequency bandwidths were included.

In addition the optimal microstructure properties in the context of sound absorption were discussed by Perrot et al., see [9–13]. Using numerical solutions of e.g. Stokes equations, appropriate parameters were calculated for given microstructures and fed into the proper macroscopic relations. They found interesting effects of throat size on absorption level, cell size in the peak absorption frequencies and fibre cross-section shape in the weight of the porous material.

The approach of the present paper explores the possible effects of altering the microscopic structure of a specific foam and the resulting acoustical properties to achieve optimal structural acoustic performance in a given application. It is apparent that the result very well may be a foam that is not presently available, but perhaps still possible to produce. Thus it is expected that this methodology may present new possibilities to predict the necessary acoustic properties and to guide in the future creation of foams that fulfil specific needs. To enable such an optimisation tool, a direct link between the foams microstructural properties and the acoustic performance is a necessity.

2. Modelling aspects

Modelling and optimising the acoustic behaviour of foams in multilayered structures requires the inclusion of several physical mechanisms representing the dynamic frequency-dependent mechanical and acoustical properties of the complex arrangement of different layers of solids, fluids and foam materials. To efficiently and accurately solve the equations governing such behaviour the finite element method is an adequate numerical solution procedure, in particular for intricate structures. However, to ensure a useful result great care has to be taken in the selection of trial solutions as well as handling the many different boundaries and interfaces within the multilayered structure. The complexity of the problem makes it computationally expensive to solve and as each frequency is solved independently, limiting the frequency range is a necessity. Furthermore, optimising the properties of one or more of the included layers requires several iterations, consequently, the optimiser's ability to find a minimum using as few iterations as possible is crucial for success.

2.1. Biot's equations

To describe the macroscopic mechanical behaviour of porous materials Biot's theory is frequently used, see e.g. [1–3]. The Biot theory describes the solid frame of the porous material and the pore fluid as an equivalent elastic solid continuum and an equivalent compressible fluid continuum, respectively. Part of Biot's theory is similar to the contemporary one presented by Zwikker and Kosten in [14] with the difference that Biot also included the effects of shear stress in the elastic frame of the porous medium. While Biot's theory is formulated for general anisotropic materials, the present work has only considered isotropic poroelastic materials. By extending Biot's theory to include internal losses and by treating the solid phase as separated from the fluid phase, the equations for the solid and fluid displacement, $\overline{u}^s$ and $\overline{u}^f$, respectively, may be written as

$$\hat{\mu}\overline{u}^s_{i,jj} + \left(\hat{\lambda} + \frac{Q^2}{R} + \hat{\mu}\right)\overline{u}^s_{j,ij} + \omega^2\rho^*\overline{u}^s_i + (\omega^2\rho_a - \mathrm{i}\omega b)(\overline{u}^s_i - \overline{u}^f_i) + Q\overline{u}^f_{j,ij} = 0 \tag{1}$$

$$R\overline{u}^f_{j,ij} + \omega^2\phi\rho_f\overline{u}^f_i + (\omega^2\rho_a - \mathrm{i}\omega b)(\overline{u}^f_i - \overline{u}^s_i) + Q\overline{u}^s_{j,ij} = 0 \tag{2}$$

Eqs. (1) and (2) assume material isotropy, small displacements and a time harmonic motion $\mathrm{e}^{\mathrm{i}\omega t}$. The constants $\hat{\mu}$, $\hat{\lambda}$, b, Q and R are complex valued material parameters which are dependent on the angular frequency ω.

The parameters $\hat{\mu}$ and $\hat{\lambda}$ represent the elastic-viscoelastic effects and are frequency-dependent analogies to Lamé's constants μ and λ. In other words, $\hat{\mu}$ and $\hat{\lambda}$ introduce frequency-dependent complex damping in the solid frame. They are thoroughly described in the augmented Hooke's law (AHL) introduced by Dovstam [15]. The acoustic-viscoacoustic effects are described by b, Q and R which are the viscous drag constant, the dilatational coupling and the pore fluid bulk modulus, respectively. Further description of the above material parameters may be found in [14,16–19].

2.2. Mechanical properties and scaling laws

In order to carry out a meaningful optimisation of the material properties of the foam, scaling laws, i.e. relations between the macroscopic properties of the foam to the underlying microscopic properties, would be required. Such scaling laws should preferably describe the macroscopic properties of the porous material as being continuously and systematically dependent on the microstructural mechanical properties. Contributions to developing scaling laws and increasing the understanding of the mechanical properties of foam have been made by several researchers.

In works by e.g. Warren and Kraynik [20,21], some mechanical properties, bulk modulus, two shear moduli and Young's modulus, are derived by analysing the stress–strain relations in repeated geometrical cell-shapes using mechanical laws. This relates the macroscopic mechanical properties to microscopic ones, e.g. Young's modulus of certain foam cell shapes to Young's modulus of the strut material and the relative density with a numerical constant that is dependent on e.g. cell shape, strut shape and joint shape. Although their work does not cover all the scaling laws needed for the current optimisation it offers a valuable insight into the microscopic behaviour of foam materials.

For simplicity the elasticity model used in the current paper is based on the work of Gibson and Ashby [22], where an isotropic open cell foam is modelled as a cubic array, see Fig. 1. The scaling laws, however, can be transferred to an arbitrary cell shape, assuming linear elastic properties in the strut material and that the struts primarily deform in bending. The following scaling laws also assume high porosity and that the strut material is significantly heavier than the interstitial fluid. The second assumption allows for the porosity, ϕ, to be expressed in terms of the bulk density of the foam, ρ^*, and the density of the strut material, ρ_s,

$$\phi = 1 - \frac{\rho^*}{\rho_s} \tag{3}$$

where ρ^*/ρ_s is the relative density. Furthermore it may be shown that the relative density is proportional to the thickness and the length of the struts forming the cells,

$$\frac{\rho^*}{\rho_s} = C^\rho\left(\frac{d_s}{l_s}\right)^2 \tag{4}$$

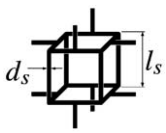

Fig. 1. Cell microstructure as assumed by Gibson and Ashby.

Finally, by simple mechanical reasoning, see [22], Young's modulus, E, can be related to the strut dimensions and consequently to the relative density

$$\frac{E^*}{E_s} = C^E\left(\frac{\rho^*}{\rho_s}\right)^2 = C^E C^\rho\left(\frac{d_s}{l_s}\right)^4 \tag{5}$$

The scaling laws have been further developed by Göransson [23]. Here relations between the microstructure and the viscous characteristic length, Λ, by Allard and Champoux [24], are used to formulate a relation for the characteristic viscous length and the static flow resistivity of the foam, σ^{static}. From Allard and Champoux, it may be deduced that assuming a pore channel with parallel walls:

$$\Lambda = \frac{1}{c_g}\sqrt{\frac{8\alpha_\infty\eta}{\phi\sigma^{\text{static}}}} \tag{6}$$

where c_g is a pore shape dependent constant that for cylindrical geometry is equal to one. η is the viscosity of air and α_∞ is the tortuosity. According to Allard the viscous characteristic length, Λ, may also be derived from the velocity field around a cylinder in an acoustic field [16]. Assuming high porosity and cylindrical struts Λ may be related to the microscopic properties as

$$\Lambda = \frac{d_s}{4(1-\phi)} = \frac{d_s}{4(\rho^*/\rho_s)} \tag{7}$$

The characteristic thermal length, Λ', was approximated as $\Lambda' = 2\Lambda$ [16]. Adopting the common assumption that the parallel duct flow model may be used for an open cell strut like foam, Eqs. (6) and (7) give

$$\sigma^{\text{static}} = \frac{8\alpha_\infty\eta}{1-(\rho^*/\rho_s)}\cdot\frac{16(\rho^*/\rho_s)^2}{c_g^2 d_s^2} \tag{8}$$

where $0<\rho^*/\rho_s<1$. Assuming high porosity, $(1-(\rho^*/\rho_s))\to 1$, constant tortuosity and by using a first-order series expansion, Eq. (8) may be simplified to

$$\sigma^{\text{static}} = \frac{C^\sigma}{d_s^2}\cdot\left(\frac{\rho^*}{\rho_s}\right)^2 \tag{9}$$

Eq. (9) represents the approximate dependence of the flow resistivity on the thickness of the struts as well as the relative density of the porous material. It is an approximation on the same level as Eq. (6) which is commonly used in analysis of open cell foam, having microstructural cell geometries far away from the original cylindrical channel that is the underlying assumption for this relation.

The constants C^ρ, C^E and C^σ are partly dependent on the microscopic mechanical properties of the foam, such as cell shape and to some extent also strut cross section shape and joint region shape. While the scaling laws by Warren and Kraynik [20,21] offers numerical values to some of these constants, they also require knowledge of cell shape, strut cross section shape and to some extent also joint region shape since these constants are dependent on those microscopic mechanical properties of the foam. Such microscopic geometrical properties may vary between different foams and are not always readily specified. The scaling laws presented in the present paper instead require a set of known macroscopic material parameters from an existing foam, as well as knowledge of the strut material properties, in order to acquire the constants C^ρ, C^E and C^σ. Provided that the material properties used to derive these constants are correct the constants will automatically, but maybe not totally, be adapted to cell shape, strut shape and joint shape. Thus, the grossly simplified cubic cell geometry will still capture the most important deformation mechanisms.

The scaling laws in Eqs. (4), (5) and (8) may also be written as

$$\rho^* = \rho_{\text{ref}}\left(\frac{d_s}{d_{\text{ref}}}\right)^2\left(\frac{l_{\text{ref}}}{l_s}\right)^2 \tag{10}$$

$$E^* = E_{\text{ref}}\left(\frac{\rho^*}{\rho_{\text{ref}}}\right)^2 \tag{11}$$

and

$$\sigma^{\text{static}} = \sigma_{\text{ref}}^{\text{static}}\left(\frac{\rho^*}{\rho_{\text{ref}}}\right)^2\cdot\left(\frac{d_{\text{ref}}}{d_s}\right)^2\cdot\frac{\alpha_\infty}{\alpha_{\infty\text{ref}}}\cdot\frac{\left(1-\frac{\rho_{\text{ref}}}{\rho_s}\right)}{\left(1-\frac{\rho^*}{\rho_s}\right)} \tag{12}$$

where Eq. (12) may be simplified into

$$\sigma^{\text{static}} = \sigma_{\text{ref}}^{\text{static}}\left(\frac{\rho^*}{\rho_{\text{ref}}}\right)^2\cdot\left(\frac{d_{\text{ref}}}{d_s}\right)^2 \tag{13}$$

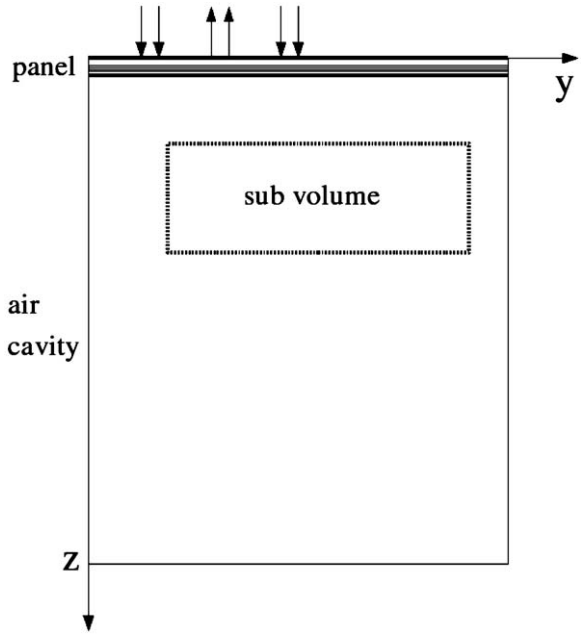

Fig. 2. Schematic picture of FE-model with coordinate system and applied forces.

using the same assumptions as for Eq. (9). The parameters ρ_{ref}, d_{ref}, l_{ref}, E_{ref}, $\sigma_{\mathrm{ref}}^{\mathrm{static}}$ and $\alpha_{\infty\mathrm{ref}}$ corresponds to the density, Young's modulus, strut thickness, strut length, static flow resistivity and tortuosity of the reference foam.

As the properties of the foam used to derive the scaling laws are comparable to the range of foam regarded in the optimisation, the scaling laws presented above, however simplified, may provide a useful tool to estimate the effect of small changes of the microscopic properties of the foam. The material properties for the porous materials used as reference materials in this paper, a polyurethane based and a polyimide based foam (PU-foam and π−foam, respectively), may be found in Appendix A. The optimisation was then performed for both these types of foam and the results are discussed below.

2.3. FE-modelling

The multilayered structures of interest in vehicle application often involve complex arrangements of different porous materials combined with purely solid or fluid layers, all with their specific boundary conditions and geometries. To calculate the acoustical mechanical response of such an intricate multilayered structure, some kind of numerical solution procedure is required. Such a numerical model must take into account not only the properties of the individual porous layers, e.g. the fluid in the pores, the solid frame structure and the coupling between them. It also has to consider the boundaries to other solid, fluid or porous layers, with appropriate treatment of the kinematic conditions, the mass flow continuity conditions and the relevant stress balances.

Additionally, special care has to be taken in the selection of trial functions to get convergent solutions to Biot's equations, especially for multilayered structures, for which hp-FEM[1] is a convenient finite element base. Here the finite element solutions were obtained using the methods thoroughly discussed and properly addressed in works by Hörlin et al. [25] and by Hörlin [26] and will not be repeated here. For completeness, however, some details of the mesh and the polynomial orders used are given below.

The analysed model is designed to describe the behaviour of an existing system where a multilayered structure acts as a roof panel for a vehicle compartment. The design of the original panel, for which several measures had already been taken to improve the NVH comfort inside the compartment, is used as a starting point and the properties of the individual sub-layers of the panel are given in Appendix B. The original design, as well as the FE-model, consists of a number of different layers intended for load carrying and/or vibration comfort purposes, with the main difference that one of the layers of the original design is a 0.01 m thick layer of air. For identification purposes, the order of the sub-layers were named as: Outer panel sheet—Air gap 1—Foam 1—Solid 1—Solid 2—Air gap 2—Interior panel sheet. The air layer named Air gap 1 is in focus for the present investigation, with the aim to illustrate microstructure optimisation in the present paper. Replacing this air layer with a layer of porous foam of equal thickness will doubtlessly incur a weight penalty. The main question is

[1] Convergence is achieved by refining the mesh and/or increasing the approximation order.

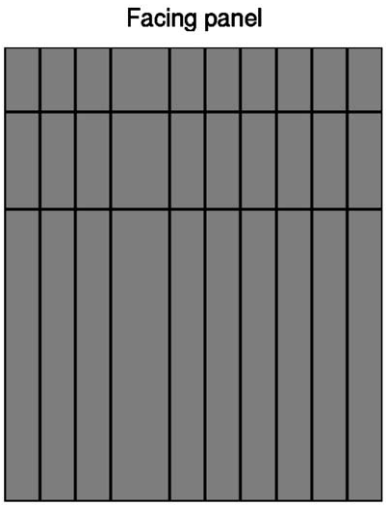

Fig. 3. Mesh of cavity FE-model with surface to panel indicated.

Table 1
Polynomial orders used in z-direction for each individual panel sub-layer, from top to bottom.

Sub-layer	Polynomial order
Outer panel sheet	4
Optimised foam	5
Foam 1	5
Solid 1	4
Solid 2	4
Air gap	2
Interior panel sheet	4

then what improvement in NVH comfort can be expected in exchange for the additional mass and, as a result of the optimisation, what is the best choice of foam to maximise the benefit of the added material?

The modelled panel, with length $L_y = 1.19$ m, consists of seven different layers where the outer and inner surfaces both have solid face sheets. The total thickness of the panel is $L_z^{\text{panel}} = 23.3$ mm and the thickness of the layer of optimised porous foam is 10 mm. The boundaries of each individual porous or solid layer of the panel at $y = 0$ and $y = L_y$ are clamped i.e. zero deflection and zero rotation whereas the boundaries between layers follow kinematic conditions and mass flow continuity requirements as mentioned previously. The outer surface of the panel is driven by three separate force fields, one out of which is 180° out of phase. Thus for $L_z = 0$, positive unit tractions were applied over: $y = 0-0.11$ m and $y = 0.51-0.62$ m; and negative unit traction over $y = 0.33-0.51$ m. The chosen force field is related to the transmission and radiation of structure borne sound, a common source of NVH problems in vehicle acoustics.

In order to enable evaluation of sound pressure levels and sound intensity the panel is connected to an air filled cavity with dimensions $L_y = 1.19$ and $L_z^{\text{cavity}} = 1.4$ m. The total length L_z is consequently $L_z = L_z^{\text{panel}} + L_z^{\text{cavity}}$ m.

For the air filled cavity there is an impedance boundary at $y = L_y$ and $z = L_z$ with a non-frequency-dependent, normal impedance equivalent to $Z = 1180 + 1044$i, which implies an absorption factor of about 50 percent. The last boundary of the air cavity, at $y = 0$, is considered to be acoustically hard (Fig. 2).

A schematic picture of the FE-model for the cavity mesh may be found in Fig. 3. Along the y-direction, a compatible mesh with 10 elements was used for the panel as well as for the cavity. For each of the sub-layers in the panel, one element through the thickness was used. In order to have a reasonably computationally efficient solution, the polynomial orders were adjusted through the different sub-layers as shown in Table 1. The polynomial orders were chosen such that the computed results had a point wise error better than 10 percent, for both displacements and pressures, at the highest frequency studied. In addition the in-plane polynomial orders were adapted to the high and low frequency ranges as discussed below.

2.4. System response

The system response was evaluated for the frequency range 100–900 Hz and the polynomial order of the base functions used to describe the porous layers was varied depending on frequency. At higher frequencies higher-order polynomials, up to 10th order, were needed to dissolve the wave pattern whereas at lower frequencies, below 600 Hz, 6th-order

polynomials were found to be sufficient. Due to the high polynomial order needed at the higher frequencies the calculation becomes very expensive. Despite this, and due to the occurrence of lowly damped acoustic cavity resonances, the frequency resolution was kept at 1 Hz all through the frequency range considered.

The sound pressure square, p_f^2, for each evaluated frequency, f, is calculated as the average of the square sound pressure in a number, N, of discrete points in a sub-volume of the air cavity, Eq. (14). The sub-volume, see Fig. 2, was chosen to represent possible ear positions of hypothetical passengers. It is bound by the following lines; $y = 0.22$ and 1.08 m, $z = 0.2233$ and 0.5233 m. In the results discussed here, N, was chosen to be 16, all points distributed in the y–z plane,

$$p_f^2 = \frac{1}{N}\sum_{n=1}^{N} p_{f_n}^2 \tag{14}$$

2.5. Formulating the optimisation problem

To compare different solutions a cost function was formulated. In the present optimisation problem either mass or sound pressure level were used, implying of course that while trying to minimise one, constraints were put on the other. In order to compare sound pressure levels over the entire frequency range the sound pressure square for each frequency were multiplied with a frequency-dependent weighting factor and a factor for frequency resolution, Δf_f, compensation and then summed over the entire frequency range. The weighting factor was chosen to correspond to either A-weighting, C_f^A, or C-weighting, C_F^C,

$$\langle \mathrm{SPL} \rangle_{\Omega_{\mathrm{sub}}}^{C} = 10 \cdot \log\left(\frac{\sum_{f=f_1}^{f_{\max}} (p_f^2 \cdot \Delta f_f \cdot C_f^C)}{p_0^2}\right) \tag{15}$$

The actual optimisation was performed with an MMA optimiser provided by Svanberg [7]. The input to the MMA optimiser consisted of the numerical values of cost function and its first and second derivate for each variable, the min- and max-values for each variable and also the numerical values of the constraint functions and their first and second derivate. The derivatives and second derivatives were calculated with finite differences and are equivalent to vectors containing the gradient and the diagonal elements of the Hessian matrix, respectively. The variables in the optimiser were chosen to be the bulk density and the strut thickness of the foam. Their respective min- and max-values were set to $8 \le \rho^* \le 70\,\mathrm{kg\,m^{-3}}$ and $10^{-7} \le d_s \le 10^{-4}$ m. These parameter ranges should be feasible and realistic for the problem at hand and furthermore lie in the range of commercially available foams. As a starting value for the strut thickness, $d_s = 10^{-5}$ m was used. For the density $15\,\mathrm{kg\,m^{-3}}$ was used.

2.5.1. Parameter space

Studies of the variation in the frequency response function obtained for varying ρ^* and d_s showed that the bulk density had a clear impact on the frequency response while the strut thickness had a much more modest effect. This was expected from previous experiences; the functional dependence between the bulk density and the flow resistivity for varying strut dimensions, described in Eq. (9) and illustrated by Göransson [23], implied that for very high porosities, above 95 percent, the bulk density indeed is the dominating parameter. For slightly lower porosity, less than 80 percent, the strut thickness becomes increasingly important for the flow resistivity, which characterises the viscous dissipation at low frequencies. The extent to which this applies may of course vary between different foams.

2.5.2. Effects of the weighting function

As described previously, weighted summation over the entire frequency range was performed in order to enable a comparison of the total sound pressure level in the sub-volume. The weighting factor corresponding to C-weighting is almost totally flat in the frequency range 100–900 Hz implying that the summed sound pressure level based on the frequency response shown in Fig. 4 would, for most ρ^*, be dominated by the sound pressure for low frequencies. On the other hand, the weighting factor corresponding to A-weighting would cause the summed SPL to be dominated by the sound pressure in high frequencies, illustrated in Fig. 5. The choice of weighting function will obviously affect the summed SPL and hence the outcome of the optimisation. Assigning a numerical value to an experienced noise, consisting of both tonal and broadband noise is an important but difficult task. The value should represent the total level of annoyance as well as other possible negative effects, a question that is often addressed in psycho-acoustics and cannot be fully investigated here. Historically the A-weighting curve is the most commonly used though it is originally meant as weighting function simulating the experienced noise level at low sound pressure levels. Whereas the B- and C-weighting is more suitable for medium high and high sound pressure levels, respectively. When measuring aircraft noise a special D-weighting is sometimes used. The D-weighting is fairly similar to the B-weighting in the frequency range 100–900 Hz. The A-, B-, C- and D-, weightings are, however, developed only based on the audible sound as it is perceived by the human ear, experienced discomfort due to structural vibrations is not at all accounted for. This raises the question of how to evaluate and compare calculations or measurements of sound pressures and vibrations in regard to acoustic NVH comfort. In short there is no obvious weighting and as in this paper, where the sound pressure is evaluated in an air filled cavity, the total sound pressure level is evaluated using two different weighting functions separately: the A-weighting and the C-weighting. This

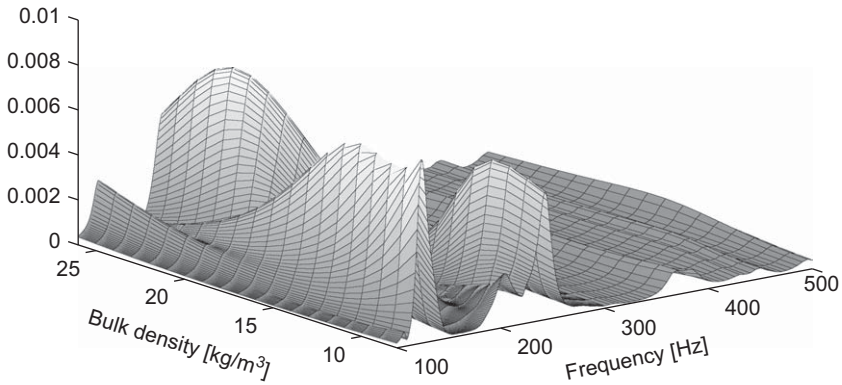

Fig. 4. Frequency response function for different ρ^* at constant $d_s = 10^{-4}$ m.

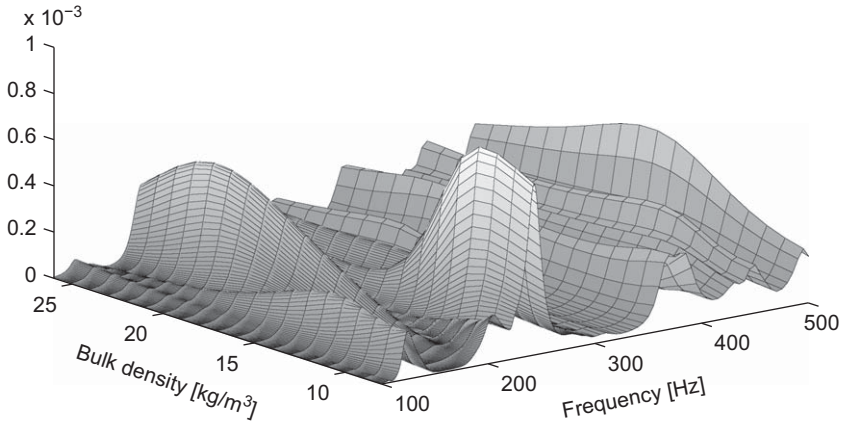

Fig. 5. Frequency response function for different ρ^* at constant $d_s = 10^{-4}$ m, multiplied with weighting factor corresponding to A-weighting.

somewhat arbitrary choice allows for a comparative evaluation of the effects of the weighting itself, not necessarily linked to the real comfort level which still remains an open issue.

2.5.3. Non-convexity

Initially it was assumed that the optimisation problem was non-convex: exhibiting a number of different minima depending on foam material and frequency range evaluated—thus different starting points were tried. However, for the single layer optimisation discussed here it was found that the number of local minima was quite limited within the parameter space and frequency range used. Thus, the choice of starting points for the optimisation turned out to be insignificant.

3. Results

Using the described method the following optimisations were performed for both the PU-foam and the $\pi-$foam: minimising the corresponding C-weighted sound pressure level with constraints on the added mass, and minimising the mass with constraints on the corresponding C-weighted sound pressure level inside the sub-volume. For the PU-foam also a minimisation of the corresponding A-weighted sound pressure level was performed in order to compare the result of using different weighting functions.

3.1. Minimising the sound pressure

In the minimisation of the sound pressure, the added mass value of the foam replacing the air gap was constrained to be 0.6 kg. For PU-foam one local minimum was found within the parameter range considered. The optimal parameters ρ^* and d_s did, however, differ depending on whether the corresponding A- or C-weighting were used.

Since adding the extra layer of foam also adds mass to the original configuration it is not sufficient to evaluate the improvement of acoustic behaviour by only comparing the frequency responses with and without foam. The mass alone

would, according to the mass law, lead to at least some transmission loss. The optimised solution with porous foam was therefore also compared with calculations of a plate with only added mass of the same amount as the foam. Finally to consider the effect of potentially sub-optimal foam a comparison was made between the best foam found and the worst foam found. Note that the worst foam found is most likely not the worst possible foam within the parameter range, only the worst that occurred during the optimisation process.

The optimal PU-foam using the corresponding A-weighting, PU^A, was found at $\rho = 32.5\,\mathrm{kg\,m^{-3}}$ and $d_s = 14.8 \times 10^{-6}\,\mathrm{m}$, which corresponds to a porosity $\phi = 0.971$, a Young's modulus $E = 138 \times 10^3\,\mathrm{Pa}$, a static flow resistivity $\sigma^{\mathrm{static}} = 662$ Rayls $\mathrm{m^{-1}}$ ($\mathrm{kg\,m^{-3}\,s^{-1}}$) and a characteristic viscous length $\Lambda = 250 \times 10^{-6}\,\mathrm{m}$. In contrast to the optimal PU-foam using the corresponding C-weighting, PU^C, was found at $\rho = 20.1\,\mathrm{kg\,m^{-3}}$ and $d_s = 15.5 \times 10^{-6}\,\mathrm{m}$, which corresponds to a porosity $\phi = 0.982$ and a Young's modulus $E = 53.0 \times 10^3\,\mathrm{Pa}$, a static flow resistivity $\sigma^{\mathrm{static}} = 233$ Rayls $\mathrm{m^{-1}}$ and a characteristic viscous length $\Lambda = 423 \times 10^{-6}\,\mathrm{m}$. The worst foam found occurred at $\rho = 12.1\,\mathrm{kg\,m^{-3}}$ and $d_s = 16.1 \times 10^{-6}\,\mathrm{m}$ for both weighting functions.

As may be seen in Table 2 the configuration with an optimised foam was significantly better than the original configuration with a layer of air, and the effect was clearly not due to added mass only but is controlled by the dynamic behaviour of the foam. The improvement caused by the added mass was very marginal which is in agreement with estimations made according to the mass law. This effect was expected and clearly visible for both cost functions used during the optimisation. What is more significant is the difference between the optimised foam and the worst foam found. This demonstrates that by adapting the foam to the specific situations, load conditions and surroundings, considerable improvements in acoustic environment may be achieved. The frequency response function for the different panel configurations may be found in Figs. 6–9.

The result and characteristics of the two optimised foams where the two different weighting factors were used showed interesting differences. The A-weighting led to a heavier and much stiffer foam, whereas the C-weighting, where the focus is more on the lower frequencies, lead to a lighter and softer foam. To further look into the possible reasons for this interesting result the displacement of the outer and inner surfaces of the panel was plotted for a number of frequencies for each of the cases. In Fig. 10 the displacements of the outer and inner surfaces at frequency 619 Hz are shown.

It is clear that a soft foam would decouple the two adjacent layer more efficiently than a stiffer one. However, many of the beneficial acoustical properties of foam will be lost when the porosity is increased. High flow resistivity is generally considered beneficial and while the flow resistivity will increase with relative density so will the stiffness and the mechanical coupling between the adjacent layers. This is also the rationale behind the current work, i.e. finding the best

Table 2
Results PU-foam for minimising A-weighted and C-weighted SPL.

Panel description	PU-foam		Configuration with air	
	Best	Worst	Original configuration	With added mass
SPL [dB(A)]	82.2	87.4	89.9	89.4
SPL [dB(C)]	87.8	90.5	94.4	94.1

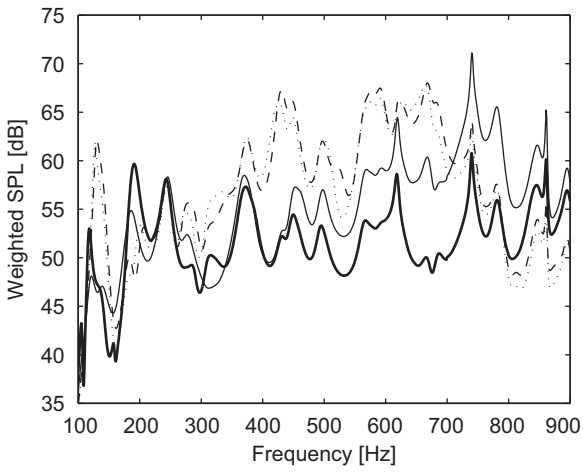

Fig. 6. Frequency response function for: optimal foam solution (thick solid), a sub-optimal foam solution (thin solid), original configuration (dashed) and original configuration with added mass (dotted), weighted with corresponding A-weighting.

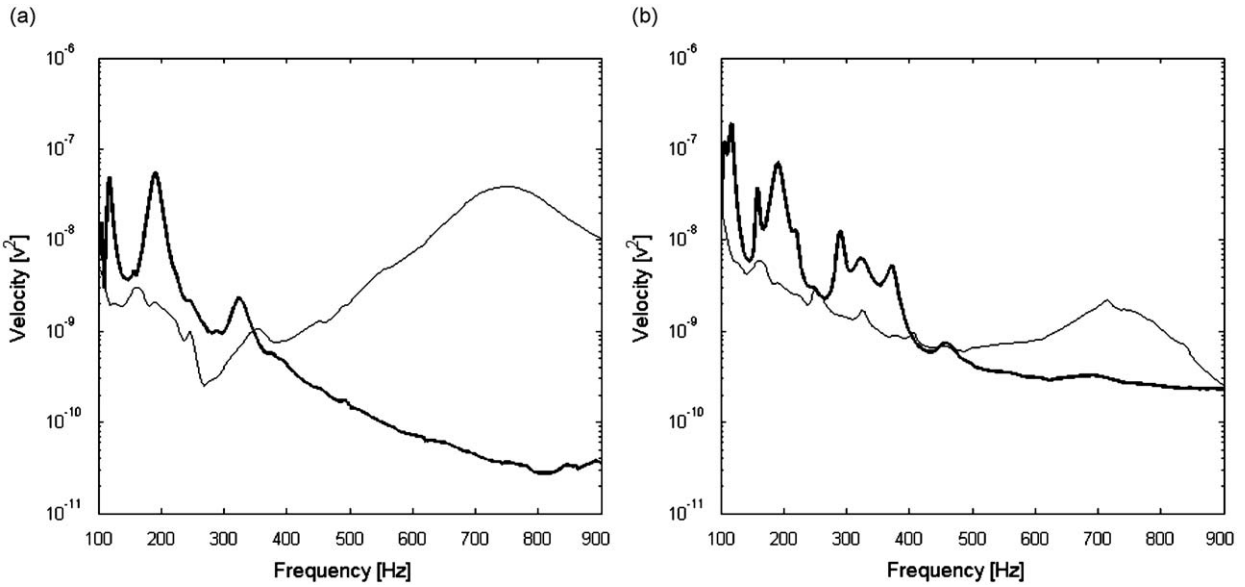

Fig. 7. Surface velocity for outer surface (a) and inner surface (b) for: A-weighted optimal foam solution (thick solid) and sub-optimal foam solution (thin solid).

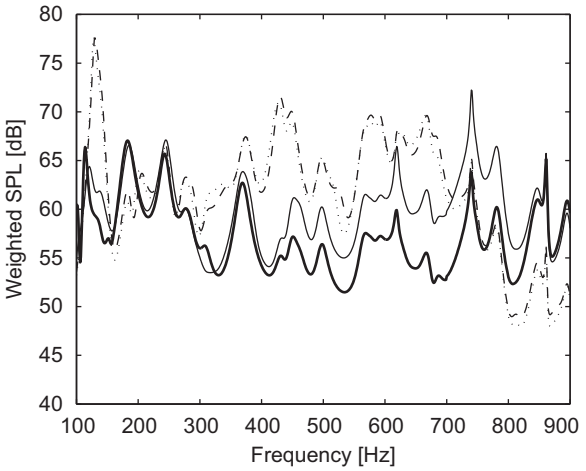

Fig. 8. Frequency response function for: optimal foam solution (thick solid), a sub-optimal foam solution (thin solid), original configuration (dashed) and original configuration with added mass (dotted), weighted with corresponding C-weighting.

balance between variables to maximise the overall benefits. Another way to understand the result from the optimisation using different weighting is in an analogy to a mass-spring system which requires a softer spring to isolate low frequencies as compared to higher frequencies. This might cause the C-weighted optimisation to result in a lower density foam; the increase of flow resistivity is not enough to compensate for the increased transmissibility of low frequency vibrations.

Optimisations were also performed trying to minimise the C-weighted SPL for the $\pi-$foam. The material forming the $\pi-$foam has a Young's modulus more than three times higher than the material forming PU-foam and is slightly heavier, about 30 percent. Such properties generally allow for thinner struts and higher porosities. The results were compared with that of the PU-foam, see Table 3 and Fig. 11. For the $\pi-$foam the minima found had a higher porosity (and lower density) compared to the PU-foam. Despite the lower density the $\pi-$foam was still significantly stiffer than the PU-foam. The frequency responses for the PU-foam and the $\pi-$foam are shown in Fig. 11. Note that the $\pi-$foam tends to be better in the high frequency range and vice versa.

An effect worth noting is that in none of the cases investigated is the optimal strut thickness found close to the minimum strut thickness allowed. Decreasing the strut thickness would increase the flow resistivity without increasing the stiffness, which may at first seem like a rational way to enhance the acoustic performance. But the dissipation of acoustic energy due to flow resistivity is dependent on the relative movement between the frame and the fluid. A great increase in flow resistivity without a corresponding increase in the stiffness may create a system where the possibility of relative

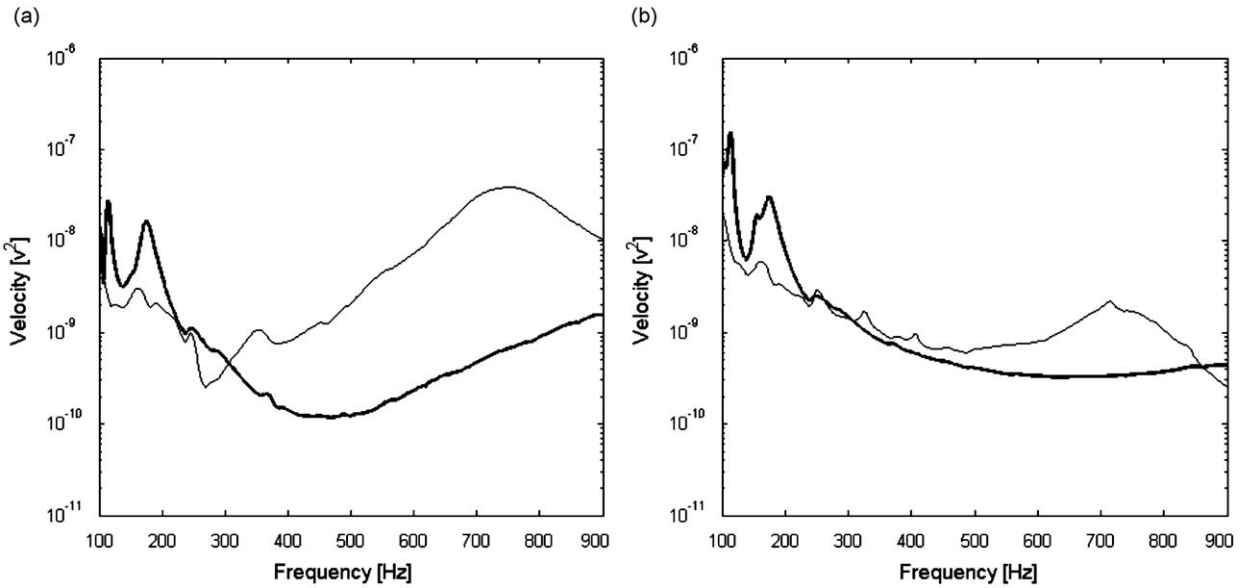

Fig. 9. Surface velocity for outer surface (a) and inner surface (b) for: C-weighted optimal foam solution (thick solid) and sub-optimal foam solution (thin solid).

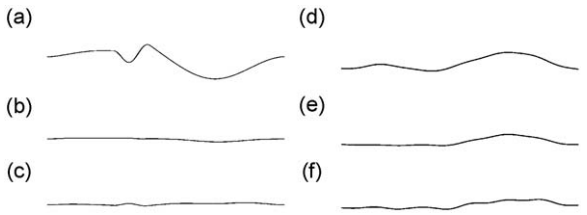

Fig. 10. Displacement of outer and inner surfaces of the multilayered panel at 619 Hz for the worst case foam found and the two optimised foam: (a) outer surface worst case foam, (b) outer surface for C-weighted optimal foam, (c) outer surface for A-weighted optimal foam, (d) inner surface worst case foam, (e) inner surface for C-weighted optimal foam, (f) inner surface for A-weighted optimal foam.

Table 3
Results for PU-foam and $\pi-$foam for minimising C-weighted SPL.

Foam	PU-foam	$\pi-$foam
SPL	87.8	88.7
ρ^*	20.1	15.3
d_s	15.5×10^{-6}	42.9×10^{-6}
ϕ	0.982	0.989
E	53.0×10^3	3121×10^3
σ^{static}	231	398
Λ	424×10^{-6}	1956×10^{-6}

motion between the frame and the fluid is greatly reduced and the waves propagating through the frame and the fluid are therefore forced to move in phase. This would most likely reduce the acoustic performance of the foam. On the contrary, in none of the cases studied is the flow resistivity particularly high. This may at first appear to be suspicious and the reason is not obvious. One possible explanation for this result may be the closed inner and outer surfaces; when air is trapped in a void with very limited possibilities of moving it will appear to be very stiff. The total thickness of the panel is 23.3 mm and some of the constant layers in the panel are either non-porous or have very high flow resistivity. So the fluid movement in z-direction is indeed quite limited. The main movement of fluid within the panel probably occurs in the y-direction, i.e. within the porous layer itself rather than between layers. Enabling good fluid movement within the porous layer may be a reason to keep the flow resistivity fairly low. As mentioned before, the relative frame-fluid motion is an important factor and adds to the dissipation of acoustic energy.

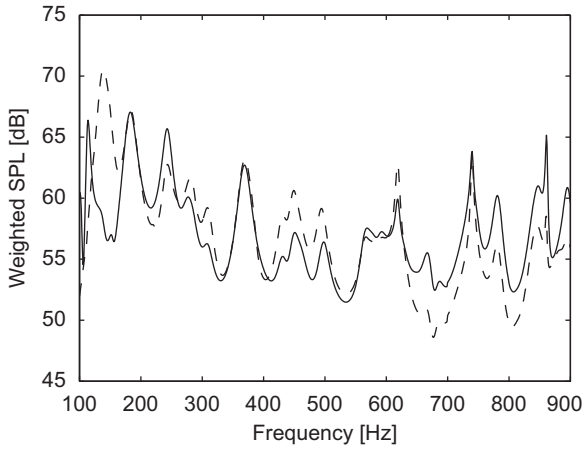

Fig. 11. Frequency response function for SPL optimised PU-foam (solid) and $\pi-$foam (dashed), weighted with corresponding C-weighting.

Table 4
Results minimising mass, constraints on C-weighted SPL.

Foam	PU-foam	$\pi-$foam
SPL	88.8	88.8
ρ^*	14.8	13.4
d_s	5.24×10^{-6}	76.7×10^{-6}
ϕ	0.987	0.990
E	28.6×10^3	2367×10^3
σ^{static}	1094	94.2
Λ	195×10^{-6}	4019×10^{-6}

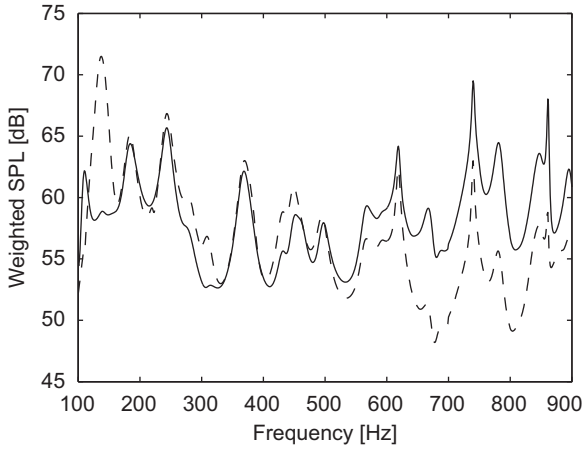

Fig. 12. Frequency response function for mass optimised PU-foam (solid) and $\pi-$foam (dashed). Maximum SPL: 88.8 dB(C), weighted with corresponding C-weighting.

3.2. Minimising the mass

When minimising the mass, constraints were placed on the C-weighted sound pressure level in the air filled cavity; the SPL was not to exceed 88.8 dB(C). Minimisation was performed for the PU foam and the $\pi-$foam using the previously found foam parameters as starting points. The result was as could have been expected: the constraint on the SPL allowed for a slightly lower density for the foam than the one found when minimising the SPL.

The results are presented in Table 4 and Fig. 12 and as can be seen the resulting densities are quite similar, though the effect is not due to the added mass. However, the rest of the foam parameters as well as the frequency responses suggest that the behaviour of the two different panels have significant differences.

4. Conclusions

Despite the limited amount of foam and layer combinations tested, the results presented above suggest realistic changes of the microscopic properties of the foam that may be sufficient to adapt the foam to a specific environmental condition and thereby achieve improved acoustic behaviour as well as reduced weight. The foam studied in this paper shows a non-convex behaviour, however, the number of minima within the parameter range seems to be limited which enables a meaningful optimisation.

These initial attempts to optimise foam on a microscopic level also show the significance of the cost function chosen to evaluate the effectiveness of the foam. By simply using different weighting factors when minimising the sound pressure levels, the optimisation gave very different results. This raises the question of how to formulate a cost function that in the best way describe the characteristics sought for. Such a cost function may include surface velocity, dissipated acoustic energy, sound power or a comparison to a frequency response spectrum chosen in advance. To further elaborate on possible cost functions it is quite possible that an effective cost function may combine one or more of the acoustical estimations above with values referring to weight and cost in some weighted constellation.

Rather than to optimise only one foam layer it would be natural to want to optimise an entire multilayered panel, where the number of layers, the thickness of each layer and the foam properties of each layer are all variables to be considered. The different layers may consist of highly diverse material types, from thin, highly viscoelastic layers to thicker weak layers. The development of new foam material with high stiffness and the ability to form extremely thin struts, 10^{-8} m, may also introduce both new difficulties and new possibilities in the area of multilayered structures.

Acknowledgements

The authors would like to gratefully acknowledge the financial support of the European project Friendcopter, Contract no. AIP3-CT-2003-502773 and the European project Smart Structures, Contract no. MRTN-CT-2006-035559.

Appendix A

The foams used in the presented work were a polyurethane foam (PU-foam), and a polyimide foam ($\pi-$foam), Table A1.

Table A1
Material properties for reference materials.

Material property	PU-foam	$\pi-$foam
ρ_s (kg m^{-3})	1100	1400
E_s (Pa)	450×10^6	1400×10^6
α_∞ [1]	1.17	1.17
ρ_0^* (kg m^{-3})	35.4	8
E_0 (Pa)	164×10^3	848×10^3
σ_0 (kg m^{-3} s^{-1})	4500	1000×10^3
Λ_0 (m)	96.1×10^{-6}	39×10^{-6}

Appendix B

The sub-layers of the panel are given in Tables B1 and B2, one for the solid layers and one for the fixed foam layer.

Table B1
Material properties for solid sub-layers.

Material property	Units	Outer panel sheet	Solid 1	Solid 2	Interior panel sheet
Density	(kg m^{-3})	750	1510	2700	362
Young's modulus	(Pa)	8600×10^9	55×10^4	69×10^9	6.52×10^9
Poisson's ratio	[1]	0.29	0.4	0.31	0.3
Thickness	(m)	0.005	0.001	0.0007	0.0036

Table B2
Material properties for foam sub-layer.

Material property	Units	Foam 1
Bulk density	($kg\,m^{-3}$)	354
Bulk Young's modulus	(Pa)	550×10^3
Poisson's ratio	[1]	0.39
Thickness	(m)	0.005
α_∞	[1]	2.2
σ^{static}	($kg\,m^{-3}\,s^{-1}$)	1×10^6
Λ	(m)	7.7×10^{-6}
Porosity	[1]	0.52

References

[1] M.A. Biot, Theory of propagation of elastic waves in a fluid saturated porous solid. I. Low frequency range, *Journal of the Acoustical Society of America* 28 (1) (1956) 168–178.
[2] M.A. Biot, Theory of propagation of elastic waves in a fluid saturated porous solid. II. Higher frequency range, *Journal of the Acoustical Society of America* 28 (2) (1956) 179–191.
[3] M.A. Biot, Theory of deformation of a porous viscoelastic anisotropic solid, *Journal of Applied Physics* 27 (3) (1956) 459–467.
[4] F. Simon, S. Pauzin, D. Biron, Optimisation of sandwich trim panels for reducing helicopter internal noise, *30th European Rotocraft Forum*, Vol. 2005, 2005, pp. 1025–1033.
[5] O. Tanneau, J.B. Casimir, P. Lamary, Optimization of multilayered panels with poroelastic components for an acoustical transmission objective, *Journal of the Acoustical Society of America* 120 (3) (2006) 1227–1238.
[6] J.S. Lee, E.I. Kim, Y.Y. Kim, J.S. Kim, Y.J. Kang, Optimal poroelastic layer sequencing for sound transmission loss maximization by topology optimization method, *Journal of the Acoustical Society of America* 122 (4) (2007) 2097–2106.
[7] K. Svanberg, The method of moving asymptotes—a new method for structural optimization, *International Journal for Numerical Methods in Engineering* 24 (1987) 359–373.
[8] F. Franco, K.A. Cunefare, M. Ruzzene, Structural-acoustic optimization of sandwich panels, *Journal of Vibration and Acoustics* 129 (3) (2007) 330–340.
[9] C. Perrot, F. Chevillotte, R. Panneton, Bottom-up approach for microstructure optimization of sound absorbing materials, *Journal of the Acoustical Society of America* 124 (2) (2008) 940–948.
[10] C. Perrot, F. Chevillotte, R. Panneton, X. Olny, Bottom-up approach for microstructure optimization of sound absorbing materials, *Invited Paper—Proceedings of the 19th International Congress on Acoustics*, ICA 2007, Madrid, Spain, 2007 (ISBN 84-87985-12-2).
[11] C. Perrot, R. Panneton, X. Olny, From microstructure to acoustic behaviour of porous materials, *Canadian Acoustics—Acoustique Canadienne* 32 (3) (2004) 18–19.
[12] X. Olny, F. Sgard, C. Perrot, R. Panneton, Microscopic and mesoscopic approaches for describing and building sound absorbing porous materials, *Proceedings of the Second TUL-ENTPE Workshop*: 187-206, 2004 (ISBN 2 86834 121 7).
[13] C. Perrot, R. Panneton, X. Olny, R. Bouchard, Mesostructural approach for characterising macroscopic parameters of open cell foams with computed microtomography, *Proceedings of the Institute of Acoustics* 25 (2003) 169–175 (ISBN 1 901656 56 X).
[14] C. Zwikker, C.W. Kosten, *Sound Absorbing Materials*, Elsevier Publishing Company, Amsterdam, 1949 (Chapters II and III).
[15] K. Dovstam, Augmented Hooke's law in frequency domain. A three dimensional material damping formulation, *International Journal of Solids and Structures* 32 (19) (1995) 2835–2852.
[16] J.F. Allard, *Propagation of Sound in Porous Media*: *Modelling Sound Absorbing Materials*, Elsevier Applied Science, 1993.
[17] D. Lafarge, P. Lemarnier, J.F. Allard, V. Tarnow, Dynamic compressibility of air in porous structures at audible frequencies, *Journal of the Acoustical Society of America* 102 (4) (1997) 1995–2006.
[18] S.R. Pride, A.F. Gangi, F.D. Morgan, Deriving the equations of motion for porous isotropic media, *Journal of the Acoustical Society of America* 92 (6) (1992) 3278–3290.
[19] D.L. Johnson, J. Koplik, R. Dashen, Theory of dynamic permeability and tortuosity in fluid-saturated porous media, *The Journal of Fluid Mechanics* 176 (1987) 379–402.
[20] W.E. Warren, A.M. Kraynik, The linear elastic properties of open cell foams, *Journal of Applied Mechanics* 55 (2) (1988) 341–346.
[21] W.E. Warren, A.M. Kraynik, Linear elastic behavior of a low-density Kelvin foam with open cells, *Journal of Applied Mechanics* 64 (4) (1997) 787–794.
[22] L.J. Gibson, M.F. Ashby, *Cellular Solids—Structure and Properties*, second ed., Cambridge University Press, Cambridge, 1997 First published by Pergamont Press Ltd., 1988.
[23] P. Göransson, Acoustic and vibrational damping in porous solids, *Philosophical Transactions of the Royal Society A* 364 (2006) 89–108.
[24] J.F. Allard, Y. Champoux, New empirical equations for sound propagation in rigid frame fibrous materials, *Journal of the Acoustical Society of America* 6 (91) (1992) 3346–3353.
[25] N.E. Hörlin, M. Nordström, P. Göransson, A 3-D hierarchical FE formulation of Biot's equations for elasto-acoustic modelling of porous media, *Journal of Sound and Vibration* 254 (4) (2001) 633–652.
[26] N.E. Hörlin, 3-D hierarchical hp-FEM applied to elasto-acoustic modelling of layered porous media, *Journal of Sound and Vibration* 285 (4) (2005) 341–363.